Polymer Driven Covalently Bonded Decahedral-Twinning of Ag Nanoparticles Prepared by ICP Enhanced Magnetron Sputtering Method

ARTICLE *in* THE JOURNAL OF PHYSICAL CHEMISTRY C · APRIL 2009

Impact Factor: 4.77 · DOI: 10.1021/jp900777h

6 AUTHORS, INCLUDING:

Qiang Chen
University of Science and Technology of C…
92 PUBLICATIONS **535** CITATIONS
SEE PROFILE

Yuefei Zhang
Beijing University of Technology
94 PUBLICATIONS **2,802** CITATIONS
SEE PROFILE

Jing Weng
Capital Medical University
11 PUBLICATIONS **85** CITATIONS
SEE PROFILE

THE JOURNAL OF PHYSICAL CHEMISTRY C

Article

Polymer Driven Covalently Bonded Decahedral-Twinning of Ag Nanoparticles Prepared by ICP Enhanced Magnetron Sputtering Method

Qiang Chen, Yuefei Zhang, Lizhen Yang, Siguang Chen, Jing Weng, and Lei Yue

J. Phys. Chem. C, **2009**, 113 (18), 7633-7638• DOI: 10.1021/jp900777h • Publication Date (Web): 14 April 2009

Polymer Driven Covalently Bonded Decahedral-Twinning of Ag Nanoparticles Prepared by ICP Enhanced Magnetron Sputtering Method

Qiang Chen,*,† Yuefei Zhang,‡ Lizhen Yang,† Siguang Chen,§ Jing Weng,|| and Lei Yue†

Laboratory of Plasma Physics and Materials, Beijing Institute of Graphic Communication, Beijing, 102600, China, Institute of Microstructure and Property of Advanced Materials, Beijing University of Technology, Beijing, 100124, China, Department of Chemistry, York University, Ontario, M1J 1P3, Canada, and School of Basic Medical Science, Captical Medical University, Beijing, 100069, China

Received: January 26, 2009; Revised Manuscript Received: March 9, 2009

In this paper, an inductively coupled plasma (ICP) enhanced magnetron sputtering (MS) method was utilized to deposit silver (Ag) nanoparticles embedded inside of simultaneously polymerized poly(ethylene oxide) (PEO) thin film. Ex situ transmission electron microscopy (TEM), selected area electron diffraction (SAED), and X-ray photoelectron spectroscopy (XPS) have been employed to elucidate the Ag nanoparticle structure, shape, and growth process during ICP enhanced MS deposition. The results showed that, when capped by polymer PEO film, the Ag nanocrystals were shaped in multiple-twinned particles (MTP) and further transformed into decahedrons held five-twinning structure with distinct twinning boundaries. The formation of particle size of Ag nanocrystalline on Si (100) surfaces was found unambiguously dependent on the ICP power, and the estimated particle size of Ag nanoparticles was in the range of 5−10 nm. From the results, it was assumed that PEO coating was the reason for inducing the formation of Ag MTP and nanodecahedron structures.

Introduction

It is well known that the optical, electronic, and biological properties of silver (Ag) nanoparticles are significantly dependent on their sizes and shapes.[1−3] In particular, at present, the oriented and shaped Ag nanoparticles have attracted intensive attention because of their specific efficiencies in bionanotechnology.[4−6] It is noted that the Ag nanoparticles in the range of 1−10 nm could vitally attach to the surface of the cell membrane, and especially for Ag nanocrystal with preferential facet of (111), it can drastically disturb bacteria's permeability and respiration functions.[7,8] Thus, the syntheses of Ag nanoparticles, the particle size and shape of which could be controlled, have been widely explored, mainly by chemical methods.[9−19] Recently, because it is a feasible operation and no post-treatment is needed, the low-temperature plasma technique has also been tried to synthesize Ag nanoparticles. For example, Ag nanoparticles with size in the scale of several nanometers were synthesized with electron-beam evaporator in ultravacuum chamber,[20] and Ag nanocrystals with preferential growth in (111) facet were obtained in magnetron sputtering plasma.[21,22] From the report,[21] the highest (111) orientated Ag nanoparticle obtained at a moderate deposition pressure presented the highest-packed structure and possessed most hydrophobic behavior. However, because of the quick aggregation and easy oxidation of Ag nanoparticles during vacuum deposition or magnetron sputtering, the controllable sizes and shapes of Ag nanoparticles were never achieved in one dry plasma process yet.[21,23]

Here, we present our primary results of Ag nanoparticles synthesized with a controllable size and shape in inductively coupled plasma (ICP) enhanced MS plasma. With this method, 5−10 nm Ag nanoparticles with certain shapes (multiple-twinned particles (MTP) to decahedron in face centered cubic nanocrystals) were synthesized by one-step plasma technique. The hypothesized mechanism for the formation of decahedron in face centered cubic nanocrystals in sputtering plasma was proposed. On the basis of our knowledge, there is no report yet regarding the deposition of Ag nanocrystal controlled particle size and shape by one-step plasma techniques, and it is the first time for the nanocrystalline growth mechanism during the sputtering process to be proposed.

Experimental Section

Figure 1 shows the schematic deposition system of the present experiments. All experiments were carried out in a bell-jar vacuum chamber, where Ar air was fed from 50 mm in distance to Ag target magnetron sputtering, and the monomer ethylene glycol dimethyl ether (CH_3O $(CH_2CH_2O)_nCH_3$, n = 2/3 EGDME) was fed by Ar carrier gas through a mass flow controller from another path near the substrate for ICP discharge and PEO polymerization. In order to avoid the poison of the sputtered target, it was mounted above the substrate, and the exhausted gas flowed directly to the pump after diffusing through the substrate. A shutter used to protect the substrate was moved after Ag target was presputtered for 5 min and the monomer flow was stable.

Before the deposition process, the chamber was initially evacuated to a pressure below 1.3×10^{-3} Pa, then refilled with Ar and re-evacuated to 1.3×10^{-3} Pa again; this process was repeated three times in order to remove the remaining O_2 in the chamber. The syntheses of Ag nanoparticles embedded composites were carried out at 0.1 Pa working pressures when the distance of target-to-substrate was kept constant at 100 mm,

* Corresponding author.
† Beijing Institute of Graphic Communication.
‡ Beijing University of Technology.
§ York University.
|| Captical Medical University.

10.1021/jp900777h CCC: $40.75
Published on Web 04/14/2009

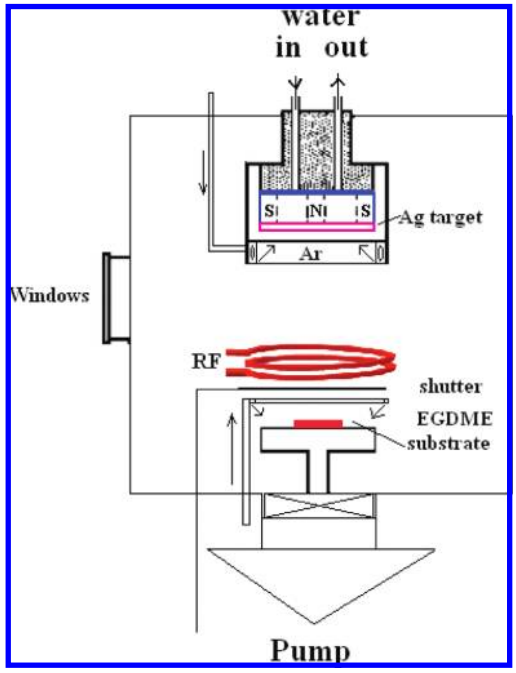

Figure 1. (Color online) Schematic diagram of the deposition system.

and target-to-middle of three-wind coil was 60 mm, whereas the Ar and monomer flow rates were kept constant.

During the sputtering processes, a DC electric source was employed for MS, and 13.56 MHz power was used for ICP discharge. The p-Si (100) wafers as substrates were cleansed ultrasonically in ethanol, acetone, and deionized water sequentially before being mounted to the sample holder. The chemical structures of the deposited nanocomposites were characterized by Fourier transform inferred (FTIR) spectroscopy (Shimadzu, FTIR-8400) and X-ray photo electron spectroscopy (XPS, Kratos Axis ULTRA, using a monochromatic Al Kα source and a charge neutralizer). The diameter and shape of Ag nanoparticles were evaluated by transmission electron microscopy (TEM, JEOL 2010F, 200 kV field emission gun). The Ag crystal facets were investigated by X-ray diffraction (XRD, Rigaku D/max-2400 with Cu Kα, radiation $\lambda = 0.154056$ nm).

Results and Discussion

Because the structure of the adding capping agent is very important for the shape of deposited Ag nanocrystal,[18,19] herewith polymerized PEO films which capped atop of Ag nanoparticles dependent on the ICP powers were investigated by FTIR, and the results are presented in Figure 1. As a comparison, the FTIR of monomer is also presented here. From Figure 1, it can be seen that a PEO film had formed,[24] and the composition of the polymerized PEO was controlled by ICP power. When ICP power increased from 10 to 30 W, the peaks around 1130 cm^{-1} assigned to C—O—C (EO) stretching band decreased sharply, and the peak shape was significantly affected and deformed; the full width half maximum (fwhm) peaks at 1130 cm^{-1} for EO group has widened in ICP enhanced MS polymerization polymers. It was found that, as the ICP power increased, the intensities of the peaks at 2950−2860 and 1460 cm^{-1} in the spectra assigned to stretching and vibration of $-CH_2$ and $-CH_3$ groups became weaker and weaker; the peaks appeared at ca. 1620 and 1200 cm^{-1} and 1030 cm^{-1} assigned to C═O, were intensified and widened, which means that the

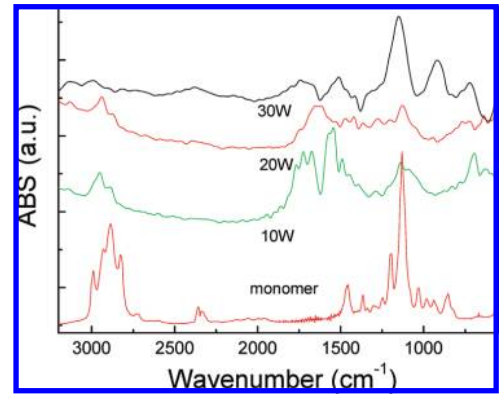

Figure 2. (Color online) FTIR spectra of Ag/PEO nanocomposites deposited in ICP enhanced MS plasma by varied the ICP powers (Ar 10 sccm, 0.1 Pa, MS 20W, 100 mm).

monomer had been severely fragmentized to form the polymer film PEO, and the compositions of polymerized PEO films have changed from having more CH_2 groups to having rich C═O groups.

Therefore, it can be concluded that, in ICP enhanced MS plasma, the PEO film was polymerized on the Ag nanoparticle surface, but the compositions of the polymer were dependent on the applied RF power.

The distribution and diameter of deposited Ag nanoparticles embedded inside of PEO films at different ICP powers were obtained from TEM images and are presented in Figure 2. From these images, one can see that the deposited Ag nanoparticles had specific homogeneous distribution in polymerized PEO films at certain ICP power, and the particle size was significantly affected by the ICP power: at lower ICP power, the diameter of particle size was increased as the ICP power increased, and when the ICP power was over 20 W, the diameter increment was limited (if we compare Figure 2b with Figure 2c, the diameter of Ag nanoparticles deposited at 20 W was seemingly in the same range as that of Ag nanoparticles deposited at 30 W), and the estimated diameter from TEM images was in the range of 5−10 nm with various shapes.

Even though TEM images of the deposited Ag nanoparticles presented in Figure 2 were in various shapes, the TEM images with higher magnification presented in Figure 3 showed that the particle shapes of whole Ag nanoparticles were mainly microstructures such as nanospheral, nanotriangle, or nanoprism. The selected area electron diffractive (SAED) pattern inserted in Figure 3a displaying the electron diffraction rings of Ag particles demonstrated unambiguously that the particles were in the nanocrystalline structure, and the discontinuous concentric ring characteristic of the Ag elucidated that Ag particles in the matrix were quite small. The nanocrystalline structure of deposited Ag particles has been confirmed in Figure 3b (marked with white arrows), in which the Ag nanoparticles more or less are crystals laid on the Si (100) substrate.

With high resolution TEM (HRTEM), the bright vertexes and five sharp edges of Ag MTP are observed distinctly in Figure 4. The five-twinning Ag shape exhibited in Figure 4a was decahedrons without perfection; it showed that an epitaxial face was grown along the bottom edge of decahedron. In Figure 4b, one can see that the coagulation took place, and the cluster was formed between decahedrons. In Figure 4c, the lattice fringes of (111) Ag planes are displayed, and the lattice spacing of the preferential orientation of (111) planes of these Ag nanocrystals is around 0.24 nm, which is in good agreement with the reported data for the face-centered cubic (fcc) Ag crystal (JCPDS No 04-0783).

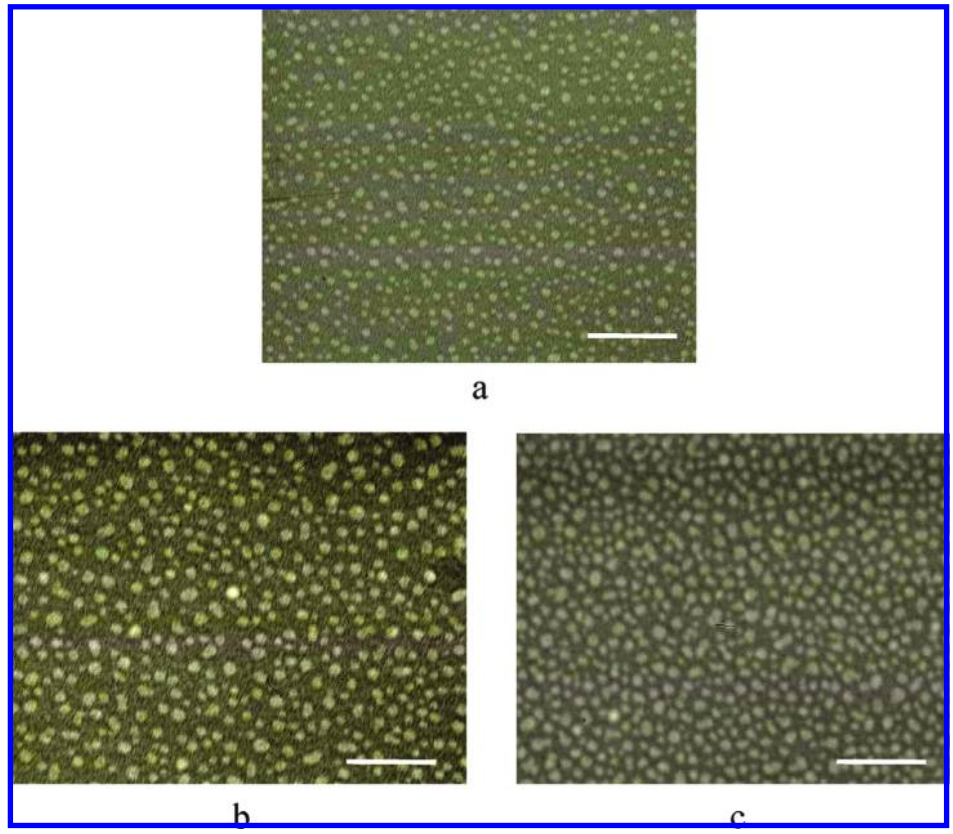

Figure 3. (Color online) TEM images of the Ag nanoparticles embedded inside of PEO films dependent on the ICP power: (a) 10 W; (b) 20 W; (c) 30 W (Ar 10 sccm, MS 20 W, the distance between substrate and target is 100 mm. The scale bar is 50 nm.)

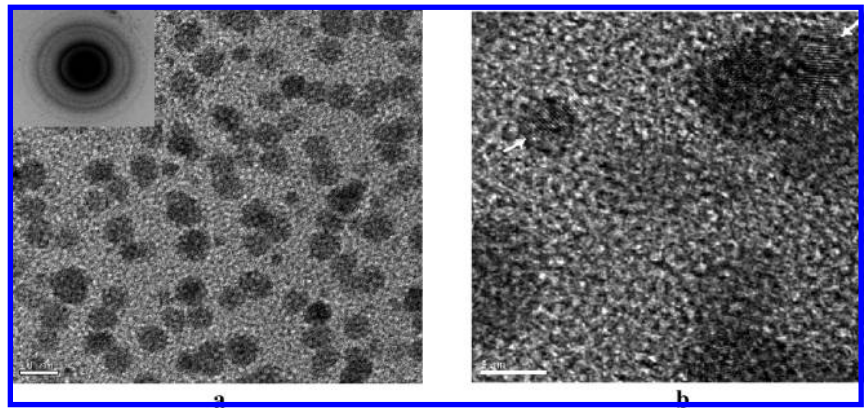

Figure 4. TEM images of the Ag nanoparticles embedded into PEO films, (a) scale 10 nm, (b) scale 5 nm (the inset is SAED. ICP 20 W, Ar 10 sccm, MS 20 W, the distance between substrate and target is 100 mm).

To confirm the preferential crystal prediction, XRD was employed to investigate the structures of ICP enhanced MS deposited Ag nanocrystals on p-Si (100) substrates, and the result is shown in Figure 5. The peaks of XRD pattern of Ag nanocrystal in Figure 5 were indexed to the diffraction of (111), (200), and (220) planes, respectively. From this XRD pattern, the crystal lattice can be calculated as 0.4076 nm, and the calculated spacing in facet (111) is 0.235 nm; it is consistent with the data obtained from HRTEM in Figure 4c. The ratio between the intensities of (111) and (200) $I_{(111)}/I_{(200)}$ is 8.3, much larger than the standard powder diffraction value of 2.4 (PCPDF No 040783); it clearly testifies that the fcc Ag nanoparticles was grown in the preferential (111) facet.

XPS had been used to further investigate the influence of ICP power on the compositions of Ag nanocrystals. Figure 6 shows the XPS spectra of the Ag nanocrystals deposited at different ICP powers in the region of 10−30 W. The peak of Ag 3d was deconvoluted in Gaussian mode and could be separated into Ag $3d_{5/2}$ and $3d_{3/2}$; the obtained binding energies of Ag $3d_{5/2}$ and $3d_{3/2}$ at different ICP powers are presented in Table 1. As comparison, the binding energies (EB) of Ag deposited without ICP (368.3 eV for Ag $3d_{5/2}$ and 374.3 eV for Ag $3d_{3/2}$[25] are also presented in Table 1.

From Figure 6 and Table 1, one can see that all BEs of 3d electrons of Ag particles deposited under ICP MS have shifted to the low energy direction; it indicates that the chemical environments around Ag atoms in the surface of the Ag nanoparticles has been changed, and as mentioned below, such kind of change was dependent on the ICP inlet power.

However, if one only compares the BEs of Ag nanoparticles deposited under ICP enhanced MS, it can be seen that the BEs of Ag 3d electrons had been increased as ICP power

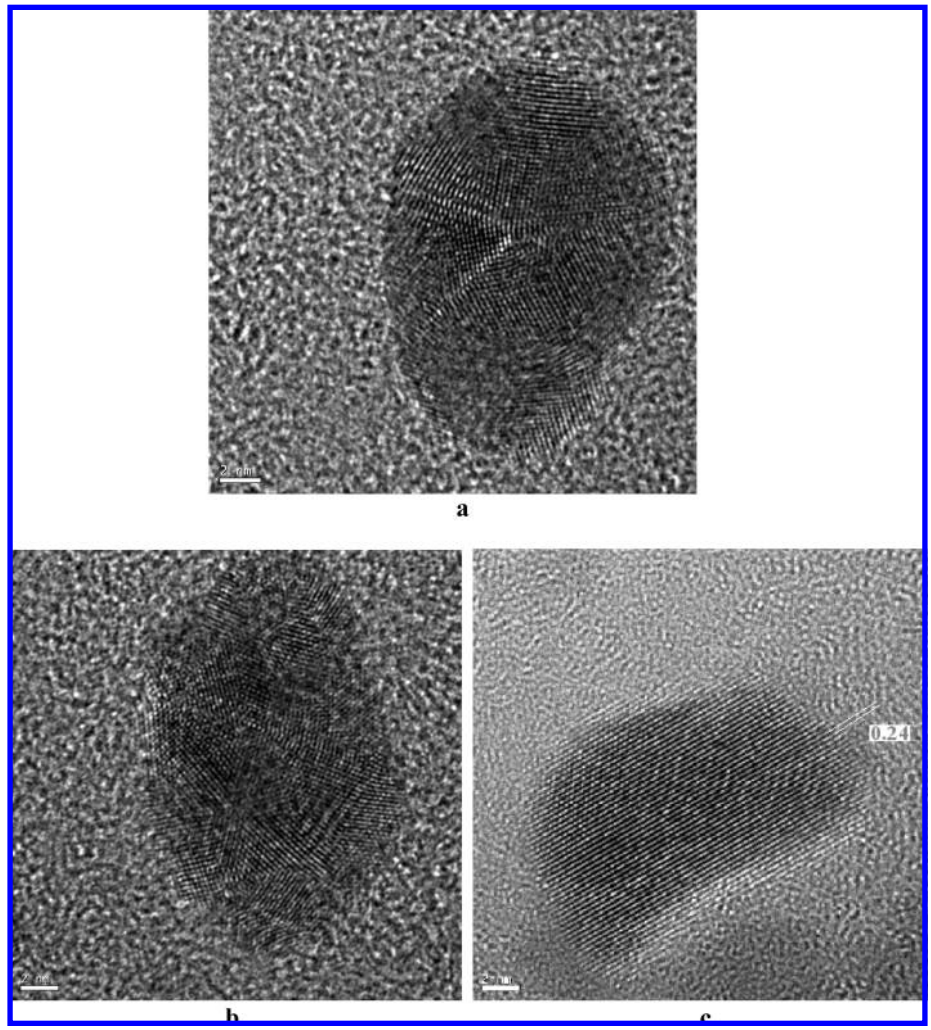

Figure 5. TEM images of the shaped Ag nanoparticles embedded into PEO matrix. (a) Decahedron. (b) Particle epitaxized from decahedron or aggregated between decahedrons. (c) Lattice fringes of (111) of Ag plane (Ar 10 sccm, MS 20 W, the distance between substrate and target is 100 mm. The scale bar is 2 nm.)

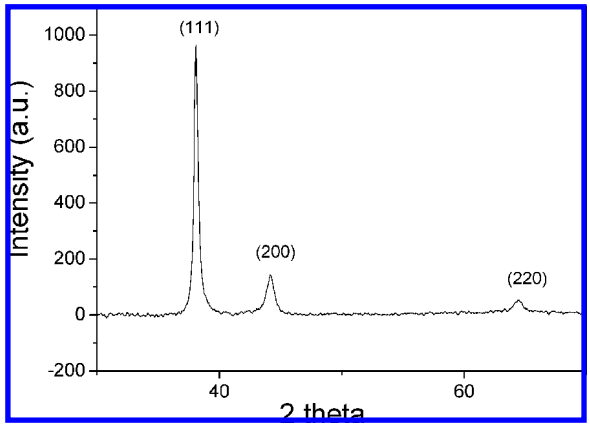

Figure 6. XRD pattern of fcc Ag nanocrystal embedded in PEO films (Ar 10 sccm, MS 20 W, ICP 20 W, 100 mm).

increasing; for example, the BE of $3d_{3/2}$ electrons increased from 373.68 to 373.84 eV, and the BE of $3d_{5/2}$ electrons increased from 367.58 to 367.74 eV when the ICP power was increased from 10 to 30 W, respectively. There was a 0.24 eV chemical blue shift for $3d_{5/2}$ electrons and a 0.16 eV shift for $3d_{3/2}$ electrons between the BEs of Ag nanoparticles deposited at 30 W ICP power and those of Ag nanoparticles deposited at 10 W ICP power. The study of the correlation between the electron BE of Ag and the particle size[26] showed that the blue shift of BE corresponded to the increase of an average domain size of Ag nanoparticles; thus, our XPS results confirmed our above TEM results that the diameters of deposited Ag nano particles increased along with the applied ICP power.

TABLE 1: EBs of Ag 3d Electrons at Different ICP Powers

	power (W)			
	0	10	20	30
EB($3d_{3/2}$) eV	374.3	373.68	373.78	373.84
EB($3d_{5/2}$) eV	368.3	367.58	367.69	367.74

We mentioned that the chemical environments of Ag atoms on top of Ag nanoparticle changed under ICP enhanced MS condition, from FTIR results. We knew that PEO films had been polymerized atop of Ag nanocrystals, because it could screen the 3d electrons of Ag atoms; therefore, the BEs of Ag nanoparticles deposited under ICP enhanced MS would be smaller than those of Ag nanoparticles deposited only in MS condition, for which the screen was absent. When Ag nanocrystals were deposited under ICP enhanced MS, as shown in FTIR spectra, the compositions of PEO films were not the same as the power increased from 10 to 30 W; it changed from having

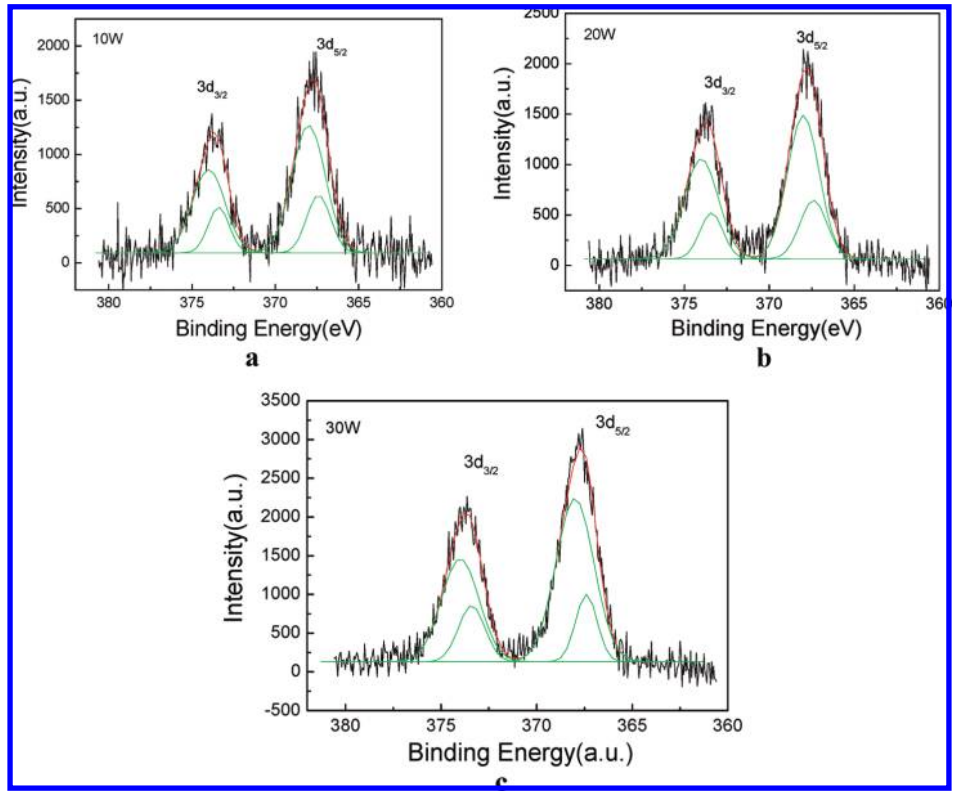

Figure 7. (Color online) XPS spectra of Ag 3d peaks for (a)10 W, (b) 20 W, and (c) 30 W deposited PEO embedded Ag nanoparticles (solid lines indicate the as-deposited, and the dot lines are simulated in Gaussian mode).

more CH_2 groups to having more C═O groups. Because the dipole moment of C═O is much higher than that of CH_2, the PEO films formed under higher ICP power would have higher polarity, and the Coulomb interaction between the PEO film and Ag 3d electrons would be higher; as a result, extra energy should be provided to remove 3d electrons from Ag atoms.[27] Therefore, 3d electrons of Ag nanoparticles deposited at higher ICP power would have higher BEs. That is the reason why the BEs of Ag nanoparticles deposited under ICP enhanced MS have a red shift compared to that of Ag nanoparticle deposited without ICP, and as ICP added MS power increased, the BEs of Ag nanoparticles deposited under ICP MS have a blue shift. Meanwhile, under ICP enhanced MS, the polymerized PEO films have the possibility to deposit on the other different facets of Ag nanoparticles; thus, it increased the growth rate along the facet (111) crystal direction.[11] In this way, the nanoparticle sizes and shapes of Ag nanocrystals could be controlled with ICP added MS method. Further studies to elucidate how the chemical structure of the PEO films controls the shapes of Ag nanocrystals in ICP enhanced MS plasma are still in progress.

Conclusion

With the ICP enhanced MS, particle size and structure controllable Ag nanocrystals embedded inside of simultaneously polymerized PEO films were synthesized. The effect of ICP power on the diameter and texture of deposited Ag nanocrystals was studied. The results showed that the diameter of formed Ag nanocrystals was determined by the ICP power, and when the power was over 20 W, the influence was relatively limited, and the growth of nanocrystals was near stable in high ICP power. The ICP power also affected the nanocrystalline shape, and the textures of deposited Ag nanocrystals varied from MTP to decahedron. A possible reason is that the facet and nanocrystal growth preferentially dominated by PEO screen and chemical composition, which shall be further studied in detail.

Acknowledgment. This work is supported by NSFC (No 1775017) and PHR (IHLB).

References and Notes

(1) Jin, R. C.; Cao, Y. W.; Mirkin, C. A.; Kelly, K. L.; Schatz, G. C.; Zheng, J. G. *Science* **2001**, *294*, 1901–1903.
(2) Peyser, L. A.; Vinson, A. E.; Bartko, A. P.; Dickson, R. M. *Science* **2001**, *291*, 103–106.
(3) Puntes, V. F.; Zanchet, D.; Erdonmez, C. K.; Alivisatos, A. P. *J. Am. Chem. Soc.* **2002**, *124*, 12874–12880.
(4) Murphy, C. J.; Jana, N. R. *Adv. Mater.* **2002**, *14*, 80–82.
(5) Chan, W. C.; Maxwell, D. J.; Gao, X. H.; Bailey, R. E.; Han, M. Y.; Nie, S. M. *Curr. Opin. Biotechnol.* **2002**, *13*, 40–46.
(6) Asharani, P. V.; Wu, Y. L. *Gong Zhiyuan and Valiyaveettil Suresh Nanotechnology* **2008**, *19*, 255102–9.
(7) Miller, R. A.; Holland, H. J. *Thin Solid Films* **1997**, *298*, 182–186.
(8) Maggioni, G.; Vomiero, A.; Carturan, S.; Scian, C.; Mattei, G.; Bazzan, M.; Fernandez, C. J.; Mazzoldi, P.; Quaranta, A.; Mea, G. D. *Appl. Phys. Lett.* **2004**, *85*, 5712–5716.
(9) Ying, C.; Chungang, W.; Zhanfang, M.; Zhongmin, S. *Nanotechnology* **2007**, *18*, 325602–325606.
(10) Sato, K.; Huang, W. J.; Bohra, F.; Sivaramakrishnan, S.; Tedjasaputra, A. P.; Zuo, J. M. *Phys. Rev. B* **2007**, *76*, 144113–144120.
(11) Gao, Y.; Jiang, P.; Song, L.; Wang, J. X.; Liu, L. F.; Liu, D. F.; Xiang, Y. J.; Zhang, Z. X.; Zhao, X. W.; Dou, X. Y.; Luo, S. D.; Zhou, W. Y.; Xie, S. S. *J. Cryst. Growth* **2006**, *289*, 376–380.
(12) Shaochun, T.; Yuefeng, T.; Shaopeng, Z.; Haiming, L.; Xiangkang, M. *J. Solid State Chem.* **2007**, *180*, 2871–2676.
(13) Hussain, S.; Roy, R. K.; Pal, A. K. *Mater. Chem. Phys.* **2006**, *99*, 375–381.
(14) Sun, Y. G.; Xia, Y. N. *Adv. Mater.* **2002**, *14*, 833–837.
(15) Hao, E.; Kelly, K. L.; Hupp, J. T.; Schatz, G. C. *J. Am. Chem. Soc.* **2002**, *124*, 15182–15183.
(16) Pastoriza-Santos, I.; Liz-Marzan, L. M. *Nano Lett.* **2002**, *2*, 903–905.
(17) Giesig, M.; Pastoriza-Santos, I.; Liz-Marzan, L. M. *J. Mater. Chem.* **2004**, *14*, 607–610.

(18) Sun, Y. G.; Xia, Y. N. *Science* **2002**, *298*, 2176–2179.
(19) Filankembo, A.; Pileni, M. P. *J. Phys. Chem. B* **2000**, *104*, 5865–5868.
(20) Li, B. Q.; Zuo, J. M. *Phys. Rev. B* **2005**, *72*, 085434–085440.
(21) Piedade, A. P.; Vieira, M. T.; Martins, A.; Silva, F. *Nanotechnology* **2007**, *18*, 105103–105107.
(22) Chiu, K.-F.; Barber, Z. H. *Thin Solid Films* **2000**, *358*, 264–269.
(23) Gangopadhyay, P.; Kesavmoorthy, R.; Bera, S.; Magudapathy, P.; Nair, K. G. M.; Panigrahi, B. K.; Narasimhan, S. V. *Phys. Rev. Lett.* **2005**, *94*, 047403–047406.
(24) Qiang, C.; Lei, Y.; Feiyan, X.; Meili, Z.; Yabo, F.; Yuefei, Z.; Jing, W. *J. Phys. Chem. C* **2008**, *112*, 10004–10007.
(25) Yan, G.; Peng, J.; Li, S.; Lifeng, L.; Xiaoqin, Y.; Zhenping, Z.; Dongfang, L.; Jianxiong, W.; Huajun, Y.; Zengxing, Z.; Xiaowei, Z.; Xinyuan, D.; Weiya, Z.; Gang, W.; Sishen, X. *J. Phys. D: Appl. Phys.* **2005**, *38*, 1061–1067.
(26) Wertheim, G. K.; Dicenzo, S. B. *Phys. ReV. B* **1988**, *37*, 844–847.
(27) Hufner S. In *Photoelectron Spectroscopy: Principles and Applications*, 2nd ed; Cardona, M., Ed.; Springer, 1996; p 32.

JP900777H